

# Emergency Landing for a Quadrotor in Case of a Propeller Failure: A Backstepping Approach

Vincenzo Lippiello, Fabio Ruggiero, and Diana Serra

**Abstract**—A backstepping approach is proposed in this paper to cope with the failure of a quadrotor propeller. The presented methodology supposes to turn off also the motor which is opposite to the broken one. In this way, a birotor configuration with fixed propellers is achieved. The birotor is controlled to follow a planned emergency landing trajectory. Theory shows that the birotor can reach any point in the Cartesian space losing the possibility to control the yaw angle. Simulation tests are employed to validate the proposed controller design.

## I. INTRODUCTION

The application of Vertical Take-off and Landing (VTOL) Unmanned Aerial Vehicles (UAVs) is moving from passive tasks like inspection and monitoring [1] into active tasks like aerial grasping [2] and manipulation [3], [4], [5], [6], [7]. This growing of interest towards service aerial robotics leads to consider controllers for safety-critical systems.

On the one hand, several techniques have been employed to control UAVs, e.g., backstepping [8], saturated nested functions [9], adaptive [10] and predictive [11] controls, and so on. On the other hand, fault detection and tolerance approaches are becoming essential due to above described changing scenario. In particular, the goal of fault tolerance methods is to maintain the same functionalities in the system even if reduced performances are present [12]. *Passive fault tolerant* systems do not alter the control structure, while *active fault tolerant* ones reconfigure the control actions [13].

Performing a literature review, on the one hand, it is possible to notice that a number of methods address the problem about controlling a quadrotor in case of motor failure by considering a partial performance loss in one or plus motors of the UAV. Supposing a 50% loss in the efficiency of a quadrotor's propeller, a method is proposed in [14] to estimate the aerial vehicle model after the failure, guaranteeing the stability of the platform. A backstepping approach is proposed in [15] but only 25% performance loss in the motors has been considered. Several methods have been compared in [16] for a 50% loss in propellers performance. A method to detect a fault is proposed in [17]. A Luenberger observer has been instead employed in [18] together with a sliding mode controller to reconfigure the controller when a partial failure appears in one motor of the

quadrotor. When the loss in the efficiency is verified in each of the four propellers, the Gain Scheduling approach in [19] can be employed. On the other hand, other methods consider the complete failure of a quadrotor's propeller. Despite the possibility to control the yaw angle, a feedback linearization with a PD-based controller is employed in [20] to control a quadrotor with a complete broken motor. A controller for an equidistant trirotor is designed in [21], but the formulation is available only for spiral motions. An H-infinity loop shaping technique is adopted in [22] for safety landing of a quadrotor with a propeller failure. Periodic solutions are exploited in [23] together with a LQR to control the quadrotor in case of single, two opposing, or three propellers failure. Recently, hexacopters are used to achieve an actuator redundancy in the system in case of failure of one or more motors.

In this paper, the failure of a quadrotor's propeller is considered, meaning that the motor is completely turned off. As assumptions, the failure has been already detected in the system, the controller has been already switched to the emergency landing modality and such trajectory has been already planned. How such things have been implemented is out of the scope of this paper: one among the techniques introduced in the literature review might be employed. Moreover, in this paper, it is considered to turn off also the motor aligned on the same quadrotor axis in which the broken propeller is placed. In this way, the resulting configuration is a *birotor* with fixed propellers<sup>1</sup>. A backstepping approach for translational movements is employed together with a PID-based control for angular displacements. Theory will show that any point in the 3D Cartesian space can be reached by the birotor, meaning that every planned emergency path can be followed. The price to pay is the impossibility to control the yaw angle since it is shown that the birotor continuously rotates around its vertical axis.

## II. MODELING

The model of a quadrotor is initially introduced. Then, the model of a birotor with fixed propellers is derived.

Define a world-fixed frame  $\Sigma_i$  and a body frame  $\Sigma_b$  placed at the center of mass of the quadrotor (see Fig. 1). The rotation of  $\Sigma_b$  with respect to  $\Sigma_i$  is denoted by the following rotation matrix  $\mathbf{R}_b(\boldsymbol{\eta}_b) \in SO(3)$  defined in [26]

$$\mathbf{R}_b(\boldsymbol{\eta}_b) = \begin{bmatrix} c_\theta c_\psi & s_\phi s_\theta c_\psi - c_\phi s_\psi & c_\phi s_\theta c_\psi + s_\phi s_\psi \\ c_\theta s_\psi & s_\phi s_\theta s_\psi + c_\phi c_\psi & c_\phi s_\theta s_\psi - s_\phi c_\psi \\ -s_\theta & s_\phi c_\theta & c_\phi c_\theta \end{bmatrix},$$

<sup>1</sup>Differently with respect to this paper, in the literature a birotor is an aerial vehicle with two propellers, whose alignment can be tilted through other two actuators [24], [25].

Authors are listed in alphabetical order. The research leading to these results has been supported by the SHERPA collaborative project, which has received funding from the European Community 7th Framework Programme (FP7/2007-2013) under grant agreements ICT-600958. The authors are solely responsible for its content.

Vincenzo Lippiello, Fabio Ruggiero and Diana Serra are with the PRISMA Lab, Department of Electrical Engineering and Information Technology, Università degli Studi di Napoli Federico II, via Claudio 21, 80125, Naples, Italy. Corresponding author's email fabio.ruggiero@unina.it.

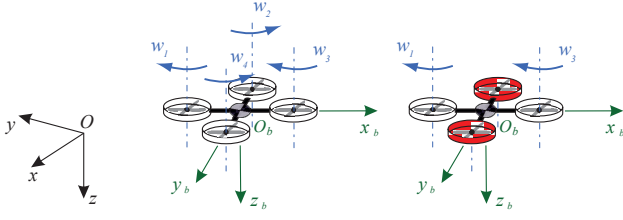


Fig. 1. On left, the quadrotor and related frames. In black the inertial frame  $\Sigma_i$ , in green the body frame  $\Sigma_b$  and in blue the speed and label of each motor. On the right, the birotor configuration with in red the turned off propellers.

in which  $s_\times$  and  $c_\times$  are employed in this paper as abbreviations for sine and cosine terms, respectively. The vector  $\boldsymbol{\eta}_b = [\phi \ \theta \ \psi]^T \in \mathbb{R}^3$  is the set of roll-pitch-yaw Euler angles denoting a minimal representation of the aerial vehicle attitude with respect to  $\Sigma_i$ . Let  $\dot{\boldsymbol{\eta}}_b = [\dot{\phi} \ \dot{\theta} \ \dot{\psi}]^T \in \mathbb{R}^3$  and  $\ddot{\boldsymbol{\eta}}_b = [\ddot{\phi} \ \ddot{\theta} \ \ddot{\psi}]^T \in \mathbb{R}^3$  be the first and second time derivatives of  $\boldsymbol{\eta}_b$ , respectively. Let  $\boldsymbol{\omega}_b^b \in \mathbb{R}^3$  the angular velocity of the quadrotor expressed in  $\Sigma_b$ . The following linear relationship holds  $\boldsymbol{\omega}_b^b = \mathbf{Q}(\boldsymbol{\eta}_b)\dot{\boldsymbol{\eta}}_b$  [27], with

$$\mathbf{Q}(\boldsymbol{\eta}_b) = \begin{bmatrix} 1 & 0 & -s_\theta \\ 0 & c_\phi & c_\theta s_\phi \\ 0 & -s_\phi & c_\theta c_\phi \end{bmatrix}.$$

Notice that the inverse relationship is defined provided that  $\theta \neq \pm\pi/2$ . Hence, it is reasonably assumed throughout all the paper that the aerial vehicle does not pass through representation singularities, meaning that the configuration space is defined as follows  $\mathcal{Q} = \{\boldsymbol{\eta}_b \in \mathbb{R}^3 : \theta \neq \pi/2 + k\pi, \phi \neq \pi/2 + k\pi, k \in \mathbb{Z}\}$ . The dynamic equations of the quadrotor can be retrieved by exploiting the Newton-Euler formulation [28]

$$m\ddot{\mathbf{p}}_b = m\mathbf{g} + \mathbf{R}_b(\boldsymbol{\eta}_b)\mathbf{f}_b^b, \quad (1a)$$

$$\mathbf{I}_b\dot{\boldsymbol{\omega}}_b^b = -\mathbf{S}(\boldsymbol{\omega}_b^b)\mathbf{I}_b\boldsymbol{\omega}_b^b - \mathbf{g}_a - \mathbf{F}_o\boldsymbol{\omega}_b^b + \boldsymbol{\tau}_b^b, \quad (1b)$$

$$\dot{\mathbf{R}}_b(\boldsymbol{\eta}_b) = \mathbf{R}_b(\boldsymbol{\eta}_b)\mathbf{S}(\boldsymbol{\omega}_b^b), \quad (1c)$$

where  $\mathbf{p}_b = [x \ y \ z]^T$ ,  $\dot{\mathbf{p}}_b = [\dot{x} \ \dot{y} \ \dot{z}]^T$ ,  $\ddot{\mathbf{p}}_b = [\ddot{x} \ \ddot{y} \ \ddot{z}]^T \in \mathbb{R}^3$  denote the absolute position, velocity and acceleration, respectively, of the aerial vehicle expressed in  $\Sigma_i$ ;  $m$  is the mass of the aerial vehicle;  $\mathbf{g} = [0 \ 0 \ g]^T \in \mathbb{R}^3$  represents the gravity vector, with  $g = 9.81 \text{ m/s}^2$ ;  $\mathbf{I}_b = \text{diag}([I_x \ I_y \ I_z]) \in \mathbb{R}^{3 \times 3}$  is the constant inertia matrix of the quadrotor expressed in  $\Sigma_b$ ;  $\mathbf{g}_a = I_p\mathbf{S}(\boldsymbol{\omega}_b^b)\mathbf{e}_3(\omega_1 + \omega_2 + \omega_3 + \omega_4)$  is the gyroscopic torques due to the combination of the aerial vehicle rotation and the propellers, with  $\omega_i$  the speed of the  $i$ th propeller,  $i = 1, \dots, 4$ , and  $I_p$  its inertia;  $\mathbf{e}_3 = [0 \ 0 \ 1]^T$  and  $\mathbf{S}(\cdot) \in \mathbb{R}^{3 \times 3}$  denotes the skew-symmetric operator;  $\mathbf{F}_o \in \mathbb{R}^{3 \times 3}$  is a diagonal positive definite matrix denoting the air friction coefficient<sup>2</sup>;  $\mathbf{f}_b^b \in \mathbb{R}^3$  and  $\boldsymbol{\tau}_b^b \in \mathbb{R}^3$  are the forces and torques input vectors, respectively, expressed in  $\Sigma_b$ .

For a quadrotor, the four control inputs are the control torques around each axis of the body frame  $\Sigma_b$  and the total

<sup>2</sup>Notice that, in general, the expression of the air drag might be more complicated depending, for instance, from the square of the velocity.

thrust  $u > 0$ , perpendicular to the propellers rotation plane. Hence, the expressions of  $\mathbf{f}_b^b$  and  $\boldsymbol{\tau}_b^b$  in (1) becomes  $\boldsymbol{\tau}_b^b = [\tau_\phi \ \tau_\theta \ \tau_\psi]^T$  and  $\mathbf{f}_b^b = [0 \ 0 \ u]^T$ . In order to design the control law on the basis of a simplified model, neglecting both the air friction terms and  $\mathbf{g}_a$  and writing the dynamic equations with respect to  $\Sigma_i$ , the model in (1) becomes [27]

$$m\ddot{\mathbf{p}}_b - m\mathbf{g} = -u\mathbf{R}_b(\boldsymbol{\eta}_b)\mathbf{e}_3, \quad (2a)$$

$$\mathbf{M}(\boldsymbol{\eta}_b)\ddot{\boldsymbol{\eta}}_b + \mathbf{C}(\boldsymbol{\eta}_b, \dot{\boldsymbol{\eta}}_b)\dot{\boldsymbol{\eta}}_b = \mathbf{Q}(\boldsymbol{\eta}_b)^T\boldsymbol{\tau}_b^b, \quad (2b)$$

with  $\mathbf{M}(\boldsymbol{\eta}_b) = \mathbf{Q}(\boldsymbol{\eta}_b)^T\mathbf{I}_b\mathbf{Q}(\boldsymbol{\eta}_b) \in \mathbb{R}^{3 \times 3}$ ,  $\boldsymbol{\eta}_b \in \mathcal{Q}$ , the symmetric and positive definite inertia matrix, and  $\mathbf{C}(\boldsymbol{\eta}_b, \dot{\boldsymbol{\eta}}_b) = \mathbf{Q}^T\mathbf{S}(\mathbf{Q}\dot{\boldsymbol{\eta}}_b)\mathbf{I}_b\mathbf{Q} + \mathbf{Q}^T\mathbf{I}_b\dot{\mathbf{Q}} \in \mathbb{R}^{3 \times 3}$  the Coriolis matrix, where  $\dot{\mathbf{Q}} \in \mathbb{R}^{3 \times 3}$  is the time derivative of  $\mathbf{Q}(\boldsymbol{\eta}_b)$ .

The total thrust  $u$  and  $\boldsymbol{\tau}_b^b$  can be related to the squared speeds  $w_i^2$ , with  $i = 1, \dots, 4$ , of the motors through [27]

$$u = \rho_u(w_1^2 + w_2^2 + w_3^2 + w_4^2), \quad (3a)$$

$$\tau_\phi = l\rho_u(w_2^2 - w_4^2), \quad (3b)$$

$$\tau_\theta = l\rho_u(w_3^2 - w_1^2), \quad (3c)$$

$$\tau_\psi = cw_1^2 - cw_2^2 + cw_3^2 - cw_4^2, \quad (3d)$$

where  $l$  is the distance between each propeller and the quadrotor's center of mass,  $\rho_u > 0$  and  $c > 0$  are two aerodynamic parameters.

Without loss of generality, suppose that motor 2 is completely broken, i.e.,  $w_2 = 0$ . Substituting this last in (3b), it is possible to notice that motor 4 creates only a negative torque around the  $x$ -axis of the aerial vehicle<sup>3</sup>. It is thus impossible to change sign to  $\tau_\phi$ . For this reason, it is assumed to turn off also motor 4, i.e.,  $w_4 = 0$ , so as to have  $\tau_\phi = 0$ <sup>4</sup>. In general, in this paper, it is proposed to turn off the motor placed on the same axis of the quadrotor where the broken propeller is located (see Fig. 1, on the right). The resulting configuration is a birotor with fixed propellers. The dynamic model of the birotor does not change with respect to (2), but the relationships in (3) differ as follows

$$u = \rho_u(w_1^2 + w_3^2), \quad (4a)$$

$$\tau_\phi = 0, \quad (4b)$$

$$\tau_\theta = l\rho_u(w_3^2 - w_1^2), \quad (4c)$$

$$\tau_\psi = cw_1^2 + cw_3^2. \quad (4d)$$

Similar equations can be obtained by considering a failure on motor 1 and/or 3. In the remainder of the paper, the aerial vehicle is referred to as a birotor with fixed propellers where, without loss of generality, motors 2 and 4 have been turned off. The case of two broken motors but not aligned on the same quadrotor's axis is out of the scope of this paper.

It is worth noticing a peculiarity of the birotor with fixed propellers:  $\tau_\psi$  in (4d) can not be freely controlled since it is impossible to change its sign. It is instead possible to

<sup>3</sup>It has been assumed that the rotational direction of each propeller is fixed, as in the most currently available off-the-shelf devices.

<sup>4</sup>The case in which all the three remaining propellers are active is considered in [23].

independently control the total thrust  $u$  and the torque  $\tau_\theta$  around the  $y$ -axis of  $\Sigma_b$ , i.e., the pitch angle. Therefore, substituting (4a) in (4d) yields

$$\tau_\psi = \bar{\tau}_\psi = cu/\rho_u, \quad (5)$$

which is the spinning torque of the birotor around its vertical axis, depending on the actual thrust and some aerodynamic parameters. Hence, the birotor continuously rotates around the  $z$ -axis of  $\Sigma_b$ .

### III. CONTROL LAW

Define the following acceleration  $\mathbf{a} = [a_x \ a_y \ a_z]^\top$  as a virtual input for the translational part of the system (2a)

$$\mathbf{a} = -(u/m)\mathbf{R}_b(\phi, \theta_d, \psi)\mathbf{e}_3 + \mathbf{g}, \quad (6)$$

where  $\theta_d$  is the desired value of the pitch angle. Vector  $\mathbf{a}$  represents the desired acceleration expressed in  $\Sigma_i$  in which the magnitude is given by the total thrust  $u$  produced by the remaining motors 1 and 3, while the attitude is given by the desired pitch angle, and the current roll and yaw angles measured by the on board IMU. By inverting (6), the retrieved values of both the thrust and the desired pitch are

$$u = m\sqrt{a_x^2 + a_y^2 + (a_z - g)^2}, \quad (7a)$$

$$\theta_d = \tan^{-1}(a_x c_\psi + a_y s_\psi / (a_z - g)). \quad (7b)$$

The goal is thus to design  $\mathbf{a}$  for the position control phase so as to compute the desired values of the thrust and the pitch angle. This last is in turn employed in a low-level control law to ensure the correct tracking of the planned angle.

- **Remark 1.** In case of a complete fault of motor 1 and/or 3, similar considerations may be done. In such a case, the desired angle is the roll, whose desired value can be computed inverting  $\mathbf{a} = -(u/m)\mathbf{R}_b(\phi_d, \theta, \psi)\mathbf{e}_3 + \mathbf{g}$  and obtaining  $\phi_d = \sin^{-1}(m(\mu_y c_\psi - \mu_x s_\psi)/u)$ .

The following subsections address separately the design of the altitude ( $a_z$ ), the planar ( $a_x$  and  $a_y$ ) and attitude ( $\theta_d$ ) controls.

#### A. Altitude control

Denote with  $\mathbf{p}_d = [x_d \ y_d \ z_d]^\top$ ,  $\dot{\mathbf{p}}_d = [\dot{x}_d \ \dot{y}_d \ \dot{z}_d]^\top$  and  $\ddot{\mathbf{p}}_d = [\ddot{x}_d \ \ddot{y}_d \ \ddot{z}_d]^\top$  the reference position, velocity and acceleration, respectively, expressed in  $\Sigma_i$ . The following PD-based controller can be employed to track the planned altitude, namely

$$a_z = \ddot{z}_d + k_{d,z}\dot{e}_z + k_{p,z}e_z, \quad (8)$$

with  $e_z = z_d - z$ ,  $\dot{e}_z = \dot{z}_d - \dot{z}$ ,  $k_{p,z}$  and  $k_{d,z}$  are positive gains. Substituting (8) in (6) and considering only the third component, it is then possible to show the asymptotic convergence of the altitude error to zero as illustrated in [27].

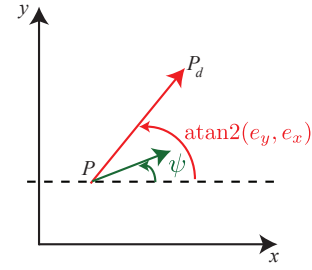


Fig. 2. The  $xy$ -plane of  $\Sigma_i$  is here represented. The point  $P$  represents the current position  $\mathbf{p}_b$  of the birotor projected in such a plane. The point  $P_d$  represents the desired position  $\mathbf{p}_d$  of the birotor on the same plane. The green vector is the current heading vector of the birotor in the  $xy$ -plane of  $\Sigma_i$ , which continuously rotates as the yaw angle. The red vector is the planar error creating an angle of  $\text{atan2}(e_y, e_x)$  with respect to the  $x$ -axis.

#### B. Planar control

As the quadrotor, the birotor is an underactuated system. In order to move in the  $xy$ -plane of  $\Sigma_i$ , the aerial vehicle has to rotate around the  $x$  or  $y$ -axis of  $\Sigma_b$  so as to create a projection vector of the vertical axis of  $\Sigma_b$  in the  $xy$ -plane of  $\Sigma_i$  allowing the planar movement.

The birotor considered here can only rotate around the  $y$ -axis of  $\Sigma_b$  and it continuously spins around  $z$ -axis. In this configuration, the projection of the birotor vertical axis into the  $xy$ -plane is a rotating vector with rate  $\dot{\psi}$  (see Fig. 2). The following kinematic constraint can be hence considered in  $\Sigma_i$

$$[\dot{x} \ \dot{y}]^\top = \mathbf{G}(\psi)v = [\cos \psi \ \sin \psi]^\top v, \quad (9)$$

where  $v$  is the magnitude of the projection vector and it is a virtual input to design in order to obtain the desired planar velocities. Since the goal is to design the desired accelerations  $a_x$  and  $a_y$ , differentiating (9) with respect to time yields

$$[a_x \ a_y]^\top = [\ddot{x} \ \ddot{y}]^\top = \dot{\mathbf{G}}(\psi, \dot{\psi})v + \mathbf{G}(\psi)\alpha, \quad (10)$$

with  $\alpha = \dot{v}$ .

Define the planar errors as  $e_x = x_d - x$  and  $e_y = y_d - y$ . Only for demonstration purposes, a regulation case, i.e.,  $\dot{x}_d = \dot{y}_d = 0$ , is here considered to design the control law. Therefore, considering the time derivatives of the planar errors and taking into account (9) yield

$$[\dot{e}_x \ \dot{e}_y]^\top = -\mathbf{G}(\psi)v, \quad (11a)$$

$$\dot{v} = \alpha, \quad (11b)$$

in which the two virtual control inputs  $\alpha$  and  $v$  have to be designed to nullify both  $e_x$  and  $e_y$ .

- **Remark 2.** Notice that the system (11) is similar to the dynamic model of a mechanical system which is subject to nonholonomic constraints: (11a) may represent the kinematic model, while (11b) may denote the so-called *dynamic extensions* [26]. The main difference is that the constraint matrix  $\mathbf{G}$  here depends on the yaw angle  $\psi$  which is an uncontrollable state variable of the system.

A backstepping approach is employed to zero the planar errors. The following theorem [29] is hence introduced.

**Theorem 1.** Consider the system (11a)-(11b). Let  $\xi(e_x, e_y)$  be a stabilizing state feedback controller for (11a) with  $\xi(0, 0) = 0$ . Let  $V(e_x, e_y)$  be a Lyapunov function satisfying

$$\frac{\partial V}{\partial [e_x, e_y]^T} \mathbf{G}(t) \xi(e_x, e_y) \leq -W(e_x, e_y), \quad (12)$$

for each value of  $e_x$  and  $e_y$ , with  $W(e_x, e_y)$  a semi-positive definite function. The following state feedback control law

$$\alpha = \frac{\partial \xi}{\partial [e_x, e_y]^T} \mathbf{G}(t) \mathbf{G}(t)^T \begin{bmatrix} \dot{e}_x \\ \dot{e}_y \end{bmatrix} - \frac{\partial V}{\partial [e_x, e_y]^T} \mathbf{G}(t) - k_b \left( \mathbf{G}(t)^T \begin{bmatrix} \dot{e}_x \\ \dot{e}_y \end{bmatrix} - \xi(e_x, e_y) \right), \quad (13)$$

marginally stabilizes the origin of system (11a)-(11b), which is  $e_x = e_y = v = 0$ , with  $k_b$  a positive gain.

*Proof.* The following state feedback control is employed to stabilize (11a)

$$v = \xi(e_x, e_y) = k_v \sqrt{e_x^2 + e_y^2} \cos(\text{atan2}(e_y, e_x) - \psi(t)), \quad (14)$$

with  $k_v$  a positive gain. Moreover, notice that  $\xi(0, 0) = 0$ . The function  $V(e_x, e_y) = (1/2)[e_x, e_y]^T [e_x, e_y]$  can be chosen as a Lyapunov function to show the stability of the point  $e_x = e_y = 0$  in (11a). By considering the time derivative of  $V(e_x, e_y)$  and the system (11a), taking into account  $e_x = \sqrt{e_x^2 + e_y^2} \cos(\text{atan2}(e_y, e_x))$  and  $e_y = \sqrt{e_x^2 + e_y^2} \sin(\text{atan2}(e_y, e_x))$  yields

$$\frac{\partial V}{\partial [e_x, e_y]^T} \mathbf{G} \xi = -k_v (e_x^2 + e_y^2) \cos^2(\text{atan2}(e_y, e_x) - \psi(t)),$$

in which dependencies have been dropped. Denoting with  $W = k_v (e_x^2 + e_y^2) \cos^2(\text{atan2}(e_y, e_x) - \psi(t))$ , it is possible to notice that this function is semi-positive definite and it is zero if and only if

$$\text{atan2}(e_y, e_x) - \psi(t) = k\pi/2, \quad (15)$$

with  $k = \pm 1, \pm 3, \pm 5, \dots$ . Inequality (12) has been then verified.

Therefore, explicitly computing (13), the following control law stabilizes the origin of system (11) as proved in [29]

$$\alpha = (\dot{e}_x(k_v + k_b) + e_x)c_\psi + (\dot{e}_y(k_v + k_b) + e_y)s_\psi + k_v k_b \sqrt{e_x^2 + e_y^2} \cos(\text{atan2}(e_y, e_x) - \psi(t)). \quad (16)$$

□

- **Remark 3.** Notice that only marginal stability is provided in Theorem 1. This is reflected in the semi-positive definiteness of the time derivative of the Lyapunov function. However, as it could be seen in Section IV, the birotor does not stuck in the condition provided by (15) due to the continuous rotation of the birotor around its vertical axis.

<sup>5</sup>This condition is verified when yaw angle  $\psi$  is at  $\pi/2$  with respect to the direction leading to  $P_d$  in the  $xy$ -plane (See Fig. 2).

### C. Pitch control

Recalling the definition of the configuration space  $\mathcal{Q}$ , the following control law can be considered for the pitch angle of the birotor

$$\tau_\theta = (I_y c_\phi + I_y s_\phi^2 / c_\phi) \bar{\tau}_\theta + \chi(\boldsymbol{\eta}_b, \dot{\boldsymbol{\eta}}_b, \bar{\tau}_\psi), \quad (17)$$

with  $\bar{\tau}_\theta$  a virtual control input and

$$\chi = I_y s_\phi (\bar{\tau}_\psi - \dot{\boldsymbol{\eta}}_b^T \mathbf{L}_1(\boldsymbol{\eta}_b) \dot{\boldsymbol{\eta}}_b) / (I_z c_\phi) + \dot{\boldsymbol{\eta}}_b^T \mathbf{L}_2(\boldsymbol{\eta}_b) \dot{\boldsymbol{\eta}}_b,$$

with

$$\mathbf{L}_1 = \begin{bmatrix} 0 & l_1 & l_2 \\ l_3 & 0 & l_4 \\ l_5 & l_6 & l_7 \end{bmatrix}, \quad \mathbf{L}_2 = \begin{bmatrix} 0 & l_8 & l_9 \\ l_{10} & 0 & l_{11} \\ l_{12} & l_{13} & l_{14} \end{bmatrix},$$

where  $l_1 = I_y c_\phi$ ,  $l_2 = I_y c_\phi s_\phi$ ,  $l_3 = -(I_x + I_z) c_\phi$ ,  $l_4 = I_x c_\phi s_\phi$ ,  $l_5 = -(I_y + I_z) c_\phi s_\phi$ ,  $l_6 = -(I_y + I_z) c_\phi s_\theta$ ,  $l_7 = (I_x - I_y) c_\phi s_\phi s_\theta$ ,  $l_8 = I_z s_\phi$ ,  $l_9 = I_x c_\phi c_\theta$ ,  $l_{10} = -(I_x + I_y) s_\phi$ ,  $l_{11} = I_x s_\phi s_\theta$ ,  $l_{12} = (I_y - I_z) c_\phi c_\theta$ ,  $l_{13} = -(I_y + I_z) s_\phi s_\theta$  and  $l_{14} = (I_z - I_x) c_\phi c_\theta s_\theta$ .

Substituting (17) in (2b) and considering (4b) and (5) yield

$$\ddot{\theta} = \bar{\tau}_\theta. \quad (18)$$

Denoting with  $\ddot{\theta}_d$ ,  $\dot{\theta}_d$  and  $\theta_d$  the desired acceleration, velocity and value of the pitch angle, respectively, the following PD-based controller can be designed

$$\bar{\tau}_\theta = \ddot{\theta}_d + k_{d,\theta} \dot{\theta} + k_{p,\theta} e_\theta, \quad (19)$$

with  $e_\theta = \theta_d - \theta$ ,  $\dot{e}_\theta = \dot{\theta}_d - \dot{\theta}$ ,  $\ddot{e}_\theta = \ddot{\theta}_d - \ddot{\theta}$ , and  $k_{p,\theta}$  and  $k_{d,\theta}$  two positive gains. Folding (19) in (18) yields the following closed-loop equation

$$\ddot{e}_\theta + k_{d,\theta} \dot{e}_\theta + k_{p,\theta} e_\theta = 0,$$

which is globally asymptotically stable.

### D. Considerations about the control scheme

In order to summarize the achieved control design, the proposed architecture is depicted in the block-scheme of Fig. 3. First, the position errors components  $e_x, e_y, e_z$  are computed, as well as the related time derivatives  $\dot{e}_x, \dot{e}_y, \dot{e}_z$ . Knowing the feedforward acceleration  $\ddot{z}_d$ , it is possible to compute the control input  $a_z$  as in (8). Taking into account both (14) and (16), the other two components of the virtual control input  $\mathbf{a}$  are retrieved as in (10). The desired total thrust  $u$  and the pitch angle  $\theta_d$  are then computed as in (7). A second-order low-pass digital filter is employed to reduce noise and compute both first and second derivatives of  $\theta_d$ . Afterwards, the pitch tracking errors  $e_\theta$  and  $\dot{e}_\theta$  are computed. The control input  $\tau_\theta$  is then retrieved as in (17), with  $\bar{\tau}_\theta$  obtained in (19). Finally, the propellers speeds for the birotor are given by (4a) and (4c). An integral action might be added in (8) and (19) to increase tracking accuracy without destroying stability properties [27].

Notice that the birotor state includes also the roll and yaw angles and their time derivatives. These quantities are not directly controlled and hence an analysis is required to check the boundedness of these variables. To roughly perform such

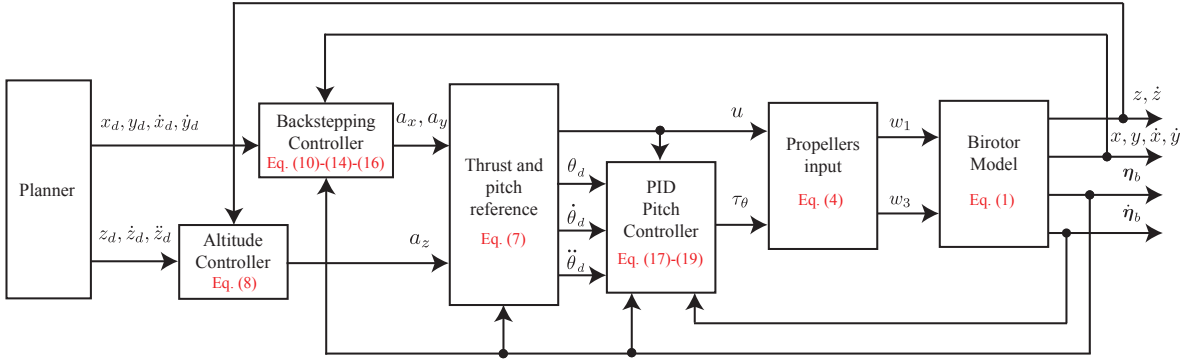


Fig. 3. Block scheme of the proposed control architecture. In red, the corresponding equations in the paper related to each block.

analysis, the Coriolis term in the dynamic model (2b) is neglected. Taking into account (4b) and (5) yields

$$\ddot{\phi} = -\frac{\sin(e_\theta - \theta_d)(I_z \tau_\theta s_\phi + I_y \bar{\tau}_\psi c_\phi)}{I_y I_z \cos(e_\theta - \theta_d)},$$

$$\ddot{\psi} = \frac{I_z \tau_\theta s_\phi + I_y \bar{\tau}_\psi c_\phi}{I_y I_z \cos(e_\theta - \theta_d)},$$

whose absolute values can be both bounded as follows by taking into account (5) and some trigonometric relationships

$$\ddot{\phi}_{max} = \ddot{\psi}_{max} = \frac{\rho_u I_z |\tau_\theta| + c I_y |u|}{\rho_u I_y I_z |\cos(e_\theta - \theta_d)|}.$$

Notice that  $\ddot{\phi}_{max}$  and  $\ddot{\psi}_{max}$  depend on the inertia, the aerodynamic parameters, the total thrust, the pitch torque, the desired pitch and the related error. The thrust can be bounded as in [27], as well as the actuated torque. Notice that the denominator is not a problem in the assumed configuration space  $\mathcal{Q}$ . For a more deep analysis, the Coriolis term should be included, but the expressions become complicated. The yaw and roll velocities can be shown to be bounded as well, but it is here omitted due to space limitation. However, the related time histories are depicted in the next section and more critical comments are provided.

#### IV. SIMULATIONS

##### A. Technical details

The proposed control law has been designed on the basis of the dynamic model (2). However, the birotor is continuously spinning around its vertical axis and then some aerodynamic effects should not be any more neglected. To properly validate the controller through simulations, the more accurate dynamic model (1) has been thus considered to simulate the aerial vehicle behaviour. Moreover, although the planar controller in Section III-B has been derived for regulation tasks, tracking cases are instead considered in the following tests.

The parameters employed in the following simulations are now introduced. Such parameters have been retrieved considering a real Asctech Pelican quadrotor [30]. The considered mass and inertia are 1.2 kg and  $\text{diag}(3.4, 3.4, 4.7) \cdot 10^{-3} \text{ kgm}^2$ , respectively. The distance of each propeller to the center of mass of the aerial vehicle is  $l = 0.21 \text{ m}$ , while the aerodynamic parameters in (4)

$\rho_u = 1.8 \cdot 10^{-5} \text{ N s}^2/\text{rad}^2$  and  $c = 8 \cdot 10^{-7} \text{ N m s}^2/\text{rad}^2$ . The inertia of the propeller is  $I_p = 3.4 \cdot 10^{-5} \text{ kgm}$ , and the term  $\mathbf{g}_a$  in (1b) for the birotor is given by  $I_p \mathbf{S}(\omega_b^b) \mathbf{e}_3 (\omega_1 + \omega_3)$ . In order to consider saturations of the actuators, a maximum speed  $w_i$  has been considered in the simulation equals to 630 rad/s (about 6000 rpm). It has been verified in the practice that the birotor at steady-state has a constant rotation speed of about 7 rad/s around its vertical axis. In this way, the friction coefficients in (1b) have been set to  $\mathbf{F}_o = \text{diag}(0, 0, 7 \cdot 10^{-2}) \text{ kgm}^2/\text{s}$ .

The gains for the altitude controller have been tuned to  $k_{p,z} = 100$ ,  $k_{d,z} = 10$  with an integral action tuned to 0.01. Concerning the backstepping controller, the gains are  $k_b = 4$  and  $k_v = 0.1$ . The gains for the pitch controller have been tuned to  $k_{p,\theta} = 64$ ,  $k_{d,\theta} = 17.6$  with an integral action tuned to 100. The sample time for acquiring measurements and giving the propellers speed has been set to 10 ms.

##### B. Case studies and discussion of the results

In the following, three case studies are described. Some other case studies can be found in the multimedia attachment. Each planned trajectory ends in the origin of  $\Sigma_i$  where the birotor stays in steady-state for few seconds. The turning off phase of the two remaining propellers is neglected.

1) *Case study A:* A diagonal emergency landing trajectory is considered in this case study. The birotor starts with an initial yaw velocity of 3 rad/s from the point  $\mathbf{p}_b = [1 \ 1 \ 1]^T \text{ m}$  in  $\Sigma_i$  and reaches the origin of the Cartesian system in 20 s. The initial and final linear velocities and accelerations are put to zero without loss of generality: a seventh-order polynomial has been employed for trajectory planning to guarantee the above defined conditions. The birotor stays for other 10 s in a steady-state condition.

The time history of the position norm is depicted in Fig. 4(a), while the pitch error is shown in Fig. 4(b). These results show also some robustness property of the proposed control law since this last has been designed on the basis of a simplified model and the theory has been provided for regulation problems. The visible oscillations are due to the continuous spinning of the birotor around its vertical axis. It has been verified that a relationship between the oscillations in the error plots and the steady-state yaw velocity exists. Notice that the yaw angle velocity is shown in Fig. 4(c),

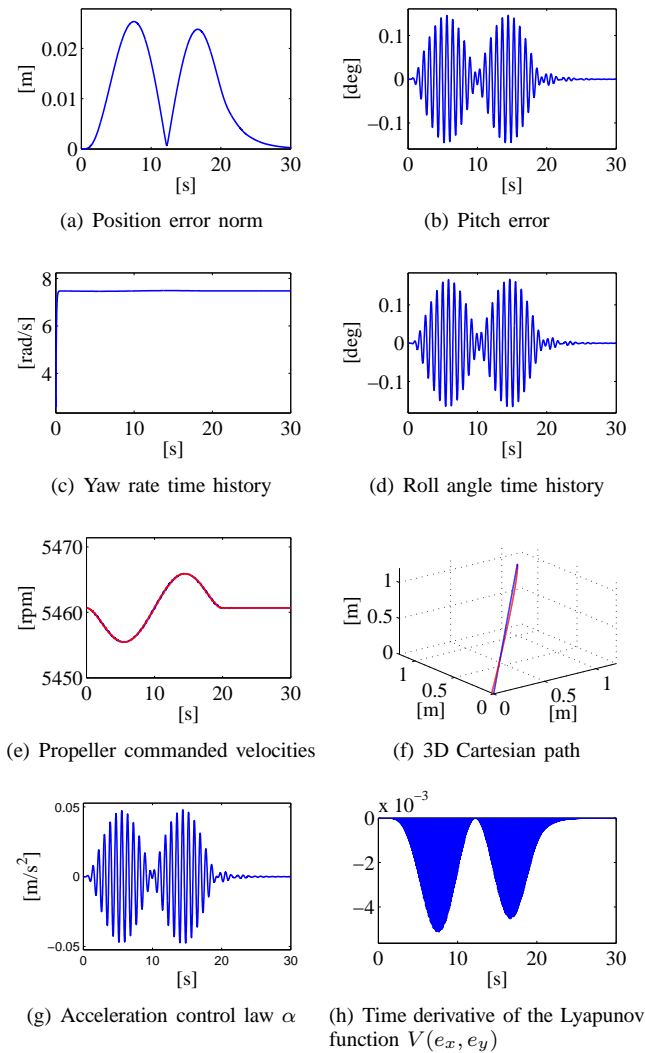


Fig. 4. Case study A: diagonal emergency landing trajectory. Subfigure (a): norm of the position error. Subfigure (b): pitch error. Subfigure (c): time history of the uncontrolled yaw angle velocity. Subfigure (d): time history of the uncontrolled roll angle. Subfigure (e): commanded velocities of the propellers. In detail, in blue the propeller 1 and in red the propeller 3. Subfigure (f): 3D Cartesian planned path. In blue the desired path, the actual one is instead depicted in red. Subfigure (g): planar acceleration control law  $\alpha$  in (16). Subfigure (h): time history of the time derivative of the Lyapunov function introduced in the proof of Theorem 1.

while the uncontrolled roll angle is depicted in Fig. 4(d) and it is limited. The commanded velocities of the propellers and the difference between planned and executed paths are shown in Fig. 4(e) and Fig. 4(f), respectively. Notice that the propeller speeds do not saturate. Fig. 4(g) shows the time history of the virtual input  $\alpha$  designed in (16). In order to show that the Lyapunov function never stops in the condition described in (15), Fig. 4(h) depicts the time history of the time derivative of the Lyapunov function  $V(e_x, e_y)$  introduced in the proof of Theorem 1. It is possible to notice that when (15) is verified, then the plot is zero. However, due to the continuous spinning of the yaw angle, its value starts again to be less than zero driving the birotor towards the desired configuration. Finally, when the planar error is zero, the time derivative of  $V(e_x, e_y)$  remains null as well.

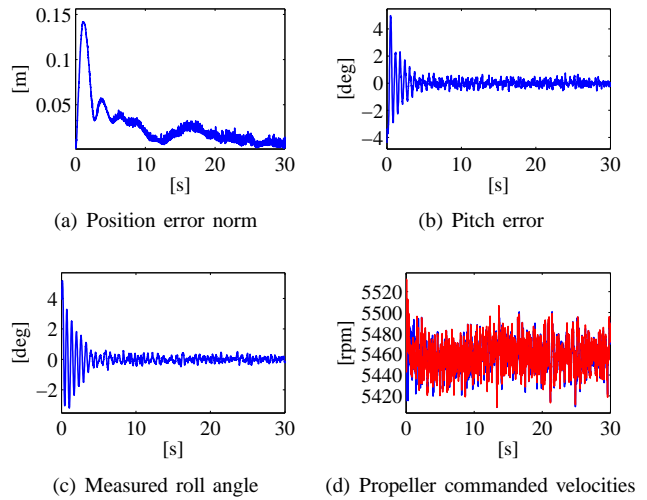


Fig. 5. Case study B: diagonal emergency landing trajectory with noise in measurement signals. Subfigure (a): norm of the position error. Subfigure (b): pitch error. Subfigure (c): measure of the uncontrolled roll angle. Subfigure (d): commanded velocities of the propellers. In detail, in blue the propeller 1 and in red the propeller 3.

2) *Case study B*: The same diagonal emergency landing trajectory of the previous case study is considered, but noise has been added to the measurement signals. In detail, white noise has been considered for the following quantities: measure of the absolute position of the birotor (variance:  $49 \cdot 10^{-6}$  m), linear velocity (variance:  $25 \cdot 10^{-4}$  m/s), IMU measure of the orientation (variance:  $3 \cdot 10^{-4}$  rad) and IMU measure of the angular velocity (variance:  $2.7 \cdot 10^{-3}$  rad/s). Moreover, it is reasonable to consider that when the fault tolerant control is switched-on, the initial conditions of both roll and pitch are not zero. In this case study, such initial values have been set to 4 deg. Time histories in Fig. 5 show that the errors remain bounded as well as the uncontrolled variables, while the propeller speeds do not saturate.

3) *Case study C*: The presence of an obstacle is considered in this case study. Hence, first a semi-circle is planned to avoid such obstacle, then a vertical straight line towards the origin of  $\Sigma_i$  is considered. The semi-circle starts at the point  $\mathbf{p}_1 = [0.5 \ 0.5 \ 1]^T$  m and passes trough  $\mathbf{p}_2 = [0.5 \ 0.5 \ 0.5]^T$  m and  $\mathbf{p}_3 = [0.5 \ 0.5 \ 0]^T$  m. The duration of this part is 20 s with initial and final linear velocity and acceleration set to zero. A seventh-order polynomial is employed for arclength parameterization for the semi-circular path. The vertical straight line has a duration of 25 s. The vehicle stays in steady-state for 5 s.

The tracking is accurate as shown in Fig. 6(a) and Fig. 6(b). Uncontrolled variables are bounded (Fig. 6(c) and Fig. 6(d)). The propeller commanded velocities, which do not saturate, and the comparison between planned and actual paths are depicted in Fig. 6(e) and Fig. 6(f), respectively.

## V. CONCLUSION AND FUTURE WORK

A backstepping controller has been designed to cope with the problem of controlling a birotor with fixed (non-tilting) propellers. This could be useful in situations where a

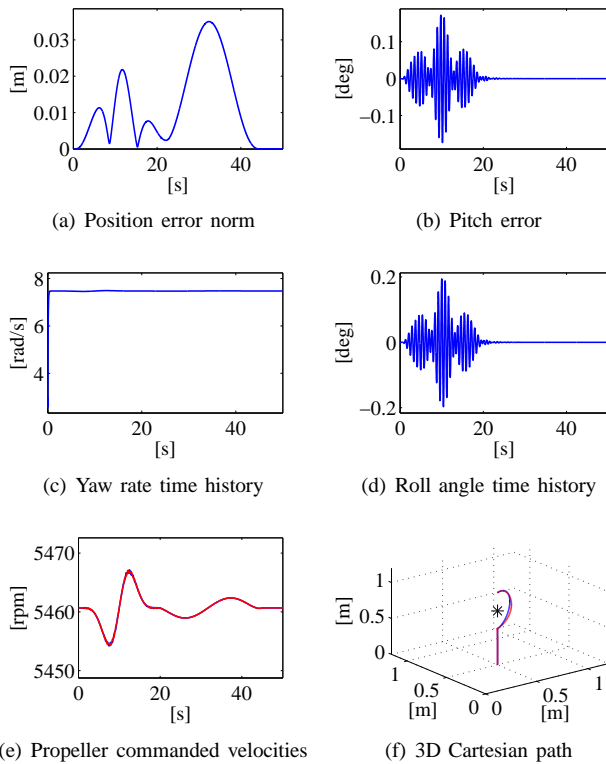


Fig. 6. Case study C: emergency landing trajectory with an obstacle. Subfigure (a): norm of the position error. Subfigure (b): pitch error. Subfigure (c): uncontrolled yaw angle velocity. Subfigure (d): uncontrolled roll angle. Subfigure (e): commanded velocities of the propellers. In detail, in blue the propeller 1 and in red the propeller 3. Subfigure (f): 3D Cartesian planned path. In blue the desired path, the actual one is depicted in red. The asterisk denotes the obstacle's position.

quadrotor completely loses one of its motor and it is assumed to turn off also the opposite actuator. The proposed approach shows that each point for Cartesian space can be reached by the birtor: each emergency landing trajectory can be thus planned. Future work is focused on experimental evaluation and problems related to an outdoor scenario.

## REFERENCES

- [1] P. Oh and W. Green, "CQAR: Closed Quarter Aerial Robot design for reconnaissance, surveillance and target acquisition tasks in urban areas," *International Journal of Computational Intelligence*, vol. 1, no. 4, pp. 353–360, 2004.
- [2] P. Pounds, D. Bersak, and A. Dollar, "Grasping from the air: Hovering capture and load stability," in *2011 IEEE International Conference on Robotics and Automation*, Shanghai, CN, 2011, pp. 2491–2498.
- [3] G. Arleo, F. Caccavale, G. Muscio, and F. Pierri, "Control of quadrotor aerial vehicles equipped with a robotic arm," in *21st Mediterranean Conference on Control and Automation*, Crete, GR, 2013.
- [4] V. Lippiello and F. Ruggiero, "Exploiting redundancy in Cartesian impedance control of UAVs equipped with a robotic arm," in *2012 IEEE/RSJ International Conference on Intelligent Robots and Systems*, Vilamoura, P, 2012, pp. 3768–3773.
- [5] R. Mebarki, V. Lippiello, and B. Siciliano, "Exploiting image moments for aerial manipulation control," in *ASME Dynamic Systems and Control Conference*, Palo Alto, CA, 2013.
- [6] R. Mebarki and V. Lippiello, "Image-based control for aerial manipulation," *Asian Journal of Control*, *Special Issue: Vision-Based Control Systems*, vol. 16, no. 3, pp. 646–656, 2014.
- [7] V. Lippiello and F. Ruggiero, "Cartesian impedance control of a UAV with a robotic arm," in *10th International IFAC Symposium on Robot Control*, Dubrovnik, HR, 2012, pp. 704–709.

- [8] S. Bouabdallah and R. Siegwart, "Full control of a quadrotor," in *2007 IEEE/RSJ International Conference on Intelligent Robots and Systems*, San Diego, CA, 2007, pp. 153–158.
- [9] P. Castillo, R. Lozano, and A. Dzul, "Stabilization of a mini rotorcraft with four rotors," *IEEE Control Systems Magazine*, vol. 25, no. 6, pp. 44–55, 2005.
- [10] G. Antonelli, F. Arrichiello, S. Chiaverini, and P. Robuffo Giordano, "Adaptive trajectory tracking for quadrotor MAVs in presence of parameter uncertainties and external disturbances," in *Proceedings 2013 IEEE/ASME International Conference on Advanced Intelligent Mechatronic*, Wollongong, AU, 2013, pp. 1337–1342.
- [11] H. Kim and D. Shim, "A flight control system for aerial robots: Algorithms and experiments," *Control Engineering Practice*, vol. 11, no. 12, pp. 1389–140, 2003.
- [12] M. Blanke, M. Staroswiecki, and N. Wu, "Concepts and methods in fault-tolerant control," in *2001 American Control Conference*, vol. 4, Arlington, VA, 2001, pp. 2606–2620.
- [13] Y. Zhang and J. Jiang, "Bibliographical review on reconfigurable fault-tolerant control systems," *Annual Reviews in Control*, vol. 32, no. 2, pp. 229–252, 2008.
- [14] M. Ranjbaran and K. Khorasani, "Fault recovery of an under-actuated quadrotor aerial vehicle," in *49th IEEE Conference on Decision and Control*, Atlanta, GA, 2010, pp. 4385–4392.
- [15] H. Khebbache, B. Sait, F. Yacef, and Y. Soukkou, "Robust stabilization of a quadrotor aerial vehicle in presence of actuator faults," *International Journal of Information Technology, Control and Automation*, vol. 2, no. 2, pp. 1–13, 2012.
- [16] Y. Zhang and A. Chamseddine, "Fault tolerant flight control techniques with application to a quadrotor UAV testbed," in *Automatic Flight Control Systems - Latest Developments*, T. Lombaerts, Ed. InTech, 2012, pp. 119–150.
- [17] A. Freddi, S. Longhi, and A. Monteri, "Actuator fault detection system for a mini-quadrotor," in *2010 IEEE International Symposium on Industrial Electronics*, Bari, I, 2010, pp. 2055–2060.
- [18] F. Sharifi, M. Mirzaei, B. Gordon, and Y. Zhang, "Fault tolerant control of a quadrotor UAV using sliding mode control," in *2010 Conference on Control and Fault-Tolerant Systems*, Nice, F, 2010, pp. 239–244.
- [19] I. Sadeghzadeh, A. Mehta, A. Chamseddine, and Y. Zhang, "Active fault tolerant control of a quadrotor UAV based on gain scheduled PID control," in *25th IEEE Canadian Conference on Electrical and Computer Engineering*, Montreal, QC, 2012, pp. 1–4.
- [20] A. Freddi, A. Lanzon, and S. Longhi, "A feedback linearization approach to fault tolerance in quadrotor vehicles," in *18th IFAC World Congress*, Milano, I, 2011, pp. 5413–5418.
- [21] Y. Kataoka, K. Sekiguchi, and M. Sampei, "Nonlinear control and model analysis of trirotor UAV model," in *18th IFAC World Congress*, Milano, I, 2011, pp. 10391–10396.
- [22] A. Lanzon, A. Freddi, and S. Longhi, "Flight control of a quadrotor vehicle subsequent to a rotor failure," *Journal of Guidance, Control, and Dynamics*, vol. 37, no. 2, pp. 580–591, 2014.
- [23] M. Mueller and R. D'Andrea, "Stability and control of a quadcopter despite the complete loss of one, two, or three propellers," in *2014 IEEE International Conference on Robotics and Automation*, Hong Kong, C, 2014, pp. 45–52.
- [24] N. Amiri, A. Ramirez-Serrano, and R. Davies, "Modelling of opposed lateral and longitudinal tilting dual-fan unmanned aerial vehicle," in *18th IFAC World Congress*, Milano, I, 2011, pp. 2054–2059.
- [25] C. Papachristos, K. Alexis, and A. Tzes, "Design and experimental attitude control of an unmanned tilt-rotor aerial vehicle," in *15th International Conference on Advanced Robotics*, Tallin, EST, 2011, pp. 465–470.
- [26] B. Siciliano, L. Sciavicco, L. Villani, and G. Oriolo, *Robotics: Modelling, Planning and Control*. London, UK: Springer, 2008.
- [27] K. Nonami, F. Kendoul, S. Suzuki, and W. Wang, *Autonomous Flying Robots. Unmanned Aerial Vehicles and Micro Aerial Vehicles*. Berlin Heidelberg, D: Springer-Verlag, 2010.
- [28] T. Hamel, R. Mahony, R. Lozano, and J. Ostrowski, "Dynamic modelling and configuration stabilization for an X4-flyer," in *15th IFAC World Congress*, Barcelona, E, 2002, pp. 846–851.
- [29] H. Khalil, *Nonlinear systems*. Upper Saddle River, NJ: Prentice Hall, 2002.
- [30] F. Ruggiero, J. Cacace, H. Sadeghian, and V. Lippiello, "Impedance control of VTOL UAVs with a momentum-based external generalized forces estimator," in *2014 IEEE International Conference on Robotics and Automation*, Hong Kong, C, 2014, pp. 2093–2099.